Обзор ArXiv/astro-ph, 7-13 октября 2025

От Сильченко О.К.

ArXiv: 2510.07407

The evolution of the bar fraction and bar lengths in the last 12 billion years

Zoe A. Le Conte,[1]★ Dimitri A. Gadotti,[1] Leonardo Ferreira,[2] Christopher J. Conselice,[3] Camila de Sá-Freitas,[4] Taehyun Kim,[5] Justus Neumann,[6] Francesca Fragkoudi,[7] E. Athanassoula,[8] and Nathan J. Adams[3]

[1]*Centre for Extragalactic Astronomy, Department of Physics, Durham University, South Road, Durham DH1 3LE, UK*
[2]*Department of Physics & Astronomy, University of Victoria, Finnerty Road, Victoria, British Columbia, V8P 1A1, Canada*
[3]*Jodrell Bank Centre for Astrophysics, University of Manchester, Oxford Road, Manchester M13 9PL, UK*
[4]*European Southern Observatory, Karl-Schwarzschild-Str. 2, D-85748 Garching bei Muenchen, Germany*
[5]*Department of Astronomy and Atmospheric Sciences, Kyungpook National University, Daegu, 41566, Republic of Korea*
[6]*Max-Planck-Institut für Astronomie, Königstuhl 17, D-69117 Heidelberg, Germany*
[7]*Institute for Computational Cosmology, Department of Physics, Durham University, South Road, Durham DH1 3LE, UK*
[8]*Aix Marseille Univ, CNRS, CNES, LAM, Marseille, France*

Accepted XXX. Received YYY; in original form ZZZ

ABSTRACT

We investigate the evolution of the bar fraction and length using an extended JWST NIRCam imaging dataset of galaxies in the $1 \leq z \leq 4$ redshift range. We assess the wavelength dependence of the bar fraction in disc galaxies and bar length evolution by selecting a nearly mass-complete CEERS disc sample and performing independent visual classifications on the short (F200W) and long (F356W+F444W) wavelength channels. A similar bar fraction is observed for both samples, and combined we find a declining trend in the bar fraction: $0.16^{+0.03}_{-0.03}$ at $1 \leq z < 2$; $0.08^{+0.02}_{-0.01}$ at $2 \leq z < 3$; $0.07^{+0.03}_{-0.01}$ at $3 \leq z \leq 4$. This corroborates our previous work and other recent studies, suggesting that dynamically cold and rotationally supported massive discs are present at Cosmic Noon. No evolution in the F356W+F444W bar length is measured from $z = 4$ to $z = 1$, which has a mean of 3.6 kpc, but a slight increase of about 1 kpc towards $z = 1$ is measured in the F200W sample, which has a mean of 2.9 kpc. The bar sample is shorter in the short-wavelength channel due to the better physical spatial resolution; however, we also suggest that dust obscuration plays a role. We find that the correlation between bar length and galaxy mass for massive galaxies observed at $z < 1$ is not seen at $z > 1$. By adding samples of barred galaxies at $z < 1$, we show that there is a modest increase in the bar length (≈ 2 kpc) towards $z = 0$, but bars longer than ≈ 8 kpc are only found at $z < 1$. We show that bars and discs grow in tandem, for the bar length normalised by disc size does not evolve from $z = 4$ to $z = 0$. Not only is a significant population of bars forming beyond $z = 1$, but our results also show that some of these bars are as long and strong as the average bar at $z \approx 0$.

Выборка

- JWST/NIRCam из архива MAST
- CEERS в двух длинах волн, F200W & (F356W+F444W)
- 1<z<4, 2438 галактик на площадке 88 кв.минут, с отрубом по массе так, чтобы на каждом красном смещении была полнота 95% (потом выборка сократилась до 520 дисковых, i<65).
- Фотометрические красные смещения взяты из CANDELS

Структурный анализ выборки

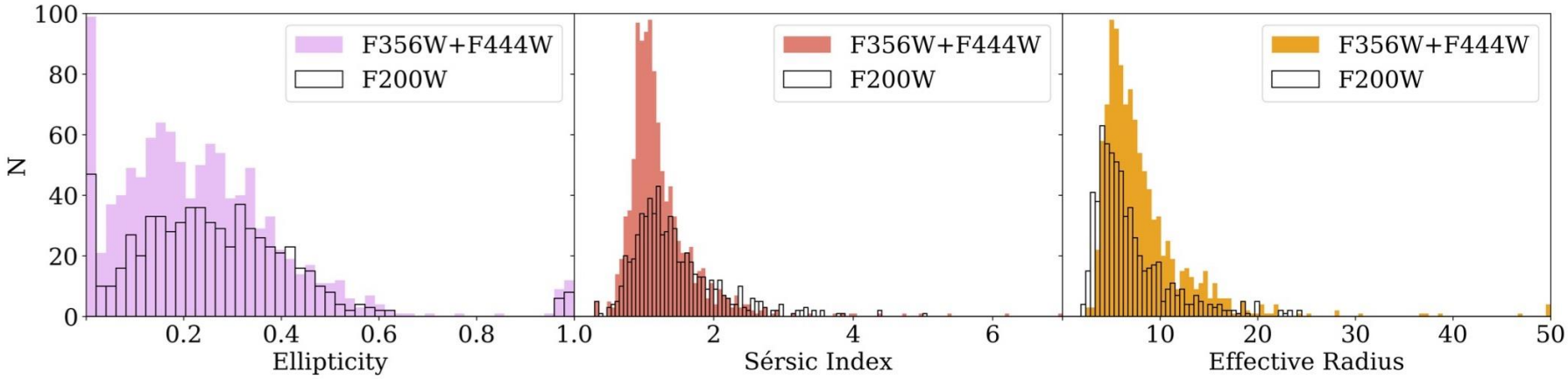

Figure 3. Distribution of the best-fit structural parameters from a single 2D Sérsic function fitting using `Imfit`, performed on the optimised samples for galaxies between $1 \leq z \leq 4$. Models fit to F356W and F444W NIRCam images are filled distributions, and those as a result of fits to F200W NIRCam images are unfilled distributions with black edges. Left: single Sérsic best-fit ellipticity, e. Middle: single Sérsic best-fit Sérsic index, n. Right: single Sérsic best-fit effective radius, r_e.

Частота встречаемости бара

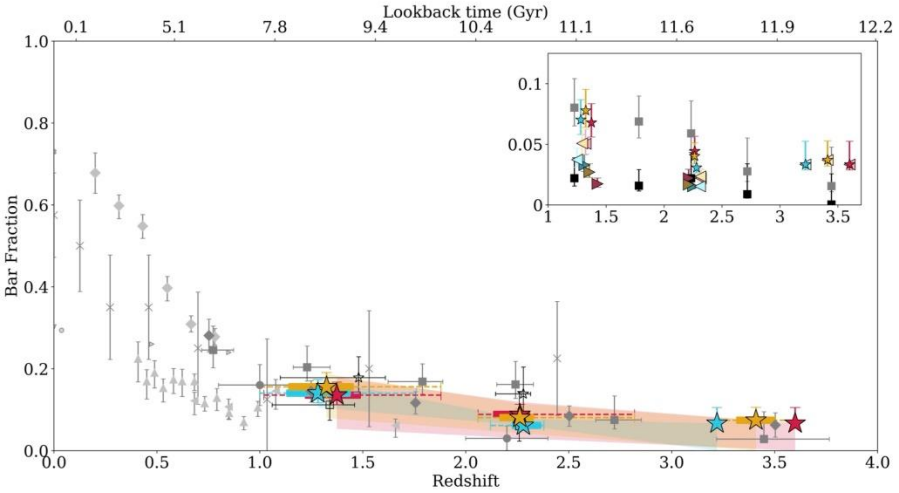

Figure 4. Evolution of the bar fraction in disc galaxies. At high-z the bar fraction is found in three redshift bins, $1 \leq z < 2$, $2 \leq z < 3$ and [illegible] the visual classification of the images from the JWST NIRCam filters F356W+F444W (red stars) and F200W (blue stars) and combining th a total bar fraction (yellow stars). Error bars in f_{bar} are the 1σ bimodal interval, and the shaded area is the upper and lower bounds of the text for details). Dashed horizontal error bars show the full range in z of the identified bars, while thick horizontal solid lines show the corresp inter-quartile range. The insert shows the bar fraction for the breakdown of strongly (right-pointing triangle) and weakly (left-pointing triangle The results of Paper 1 are black unfilled squares (HST) and stars (JWST), and in grey are the JWST bar fraction of G25 (diamond), ES25 (circle (square).

Redshift	Bar Fraction								
	F200W			F356W+F444W			F200W+F356W+F444W		
	SB	WB	B	SB	WB	B	SB	WB	B
$1 \leq z < 2$	$0.07^{+0.02}_{-0.01}$	$0.07^{+0.02}_{-0.01}$	$0.14^{+0.03}_{-0.02}$	$0.03^{+0.01}_{-0.01}$	$0.10^{+0.02}_{-0.02}$	$0.14^{+0.03}_{-0.02}$	$0.05^{+0.01}_{-0.01}$	$0.10^{+0.02}_{-0.02}$	$0.16^{+0.03}_{-0.03}$
$2 \leq z < 3$	$0.03^{+0.01}_{-0.01}$	$0.03^{+0.01}_{-0.01}$	$0.06^{+0.02}_{-0.01}$	$0.04^{+0.01}_{-0.01}$	$0.04^{+0.01}_{-0.01}$	$0.09^{+0.02}_{-0.01}$	$0.03^{+0.01}_{-0.01}$	$0.05^{+0.01}_{-0.01}$	$0.08^{+0.02}_{-0.01}$
$3 \leq z \leq 4$	-	$0.07^{+0.04}_{-0.01}$	$0.07^{+0.04}_{-0.01}$	-	$0.07^{+0.04}_{-0.01}$	$0.07^{+0.04}_{-0.01}$	-	$0.07^{+0.03}_{-0.01}$	$0.07^{+0.03}_{-0.01}$

Table 1. The bar fraction for the visually classified samples in F200W, F356W+F444W and F200W+F356W+F444W in three redshift bins. The f_{bar} is presented for strongly barred galaxies (SB), weakly barred (WB) and all barred galaxies (B). No strongly barred galaxies were found beyond $z = 3$. The errors presented are the statistical 1σ bimodal interval (see text for details).

Зависимость от массы

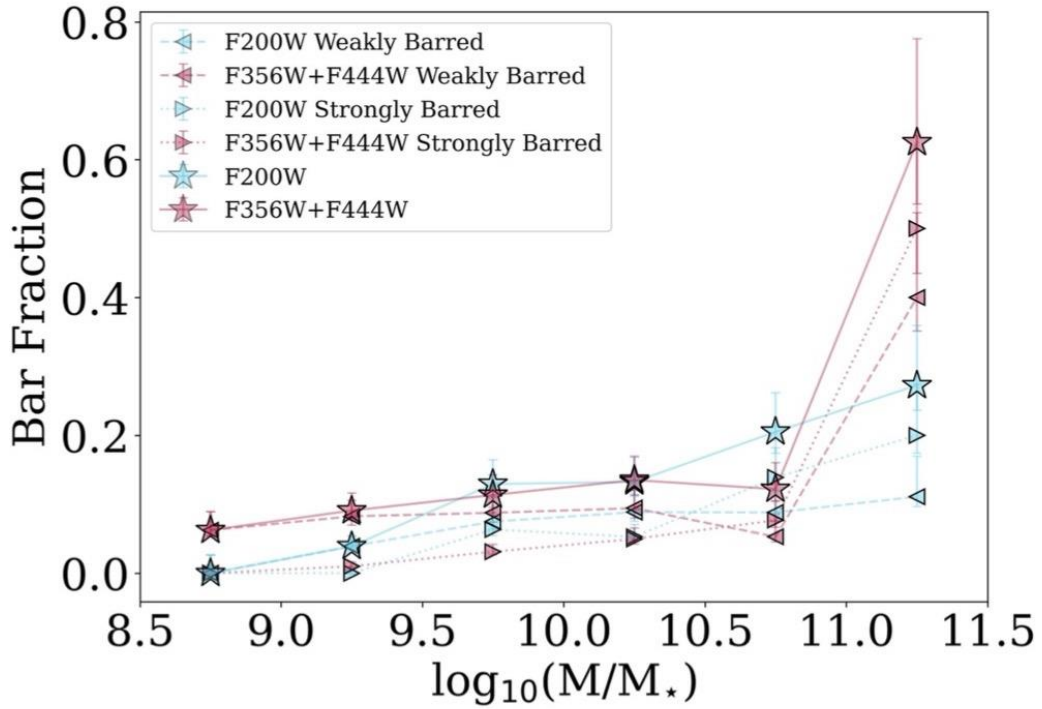

Figure 6. The fraction of bars in disc galaxies for a given stellar mass in the range $8.5 \leq \log(M_\star/M_\odot) \leq 11.5$. We show results for the NIRCam filters F200W (blue) and F356W+F444W (red). Three different samples are shown: weakly barred (left-pointing triangle); strongly barred (right-pointing triangle), and the sum of both weakly and strongly barred galaxies (star). Error bars in f_{bar} show the 1σ bimodal interval.

Длина бара

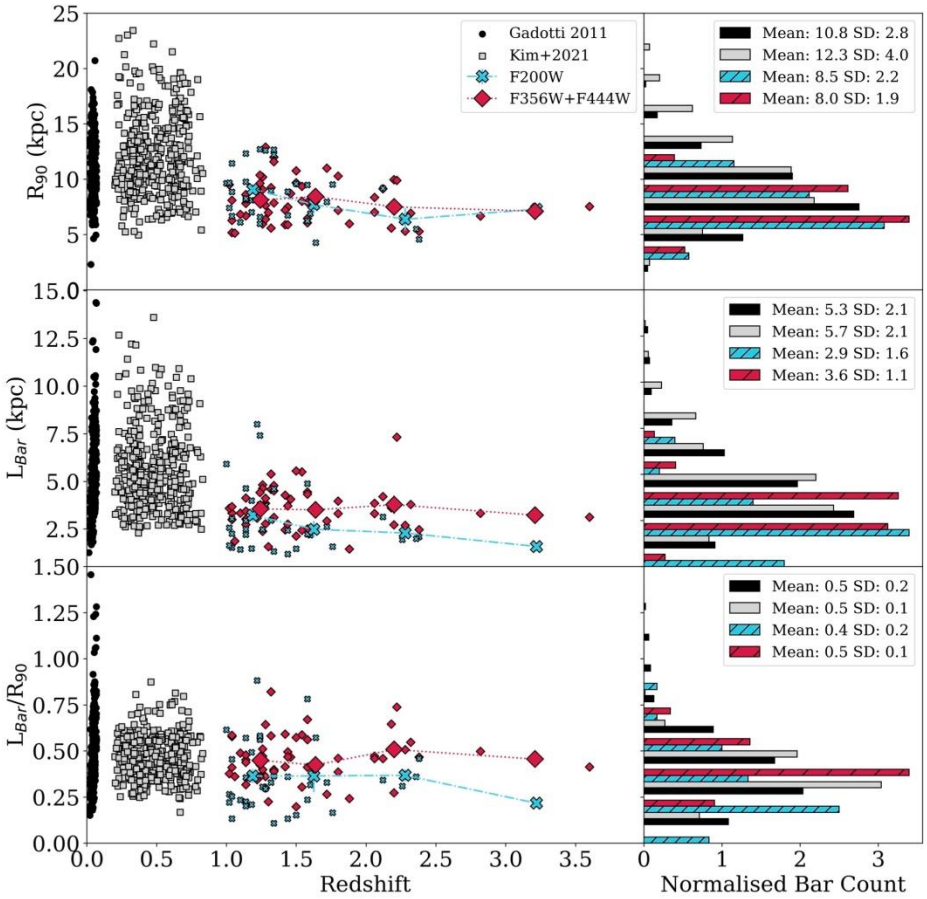

Figure 7. The evolution of the bar length over $0 \leq z \leq 4$. The left panels show lengths measured in this work from JWST NIRCam filters F200W (blue) and F356W+F444W (red) for bars found in galaxies between the redshift range $1 \leq z \leq 4$, with their normalised distribution (see text for details) shown on the right panels. The first row shows the distribution of R_{90}, whilst the second row is the deprojected L_{bar} and the third row is the normalised L_{bar}, L_{bar}/R_{90}. The high redshift sample is compared against a sample of SDSS $i-$band barred galaxies at $z \approx 0$ (G11, black) and a sample of barred galaxies at $0.2 < z \leq 0.835$ using F814W images from the COSMOS survey (K21, grey). The mean value for each parameter in each sample is given in the right panel, with the standard deviation.

Пример зависимости от длины волны

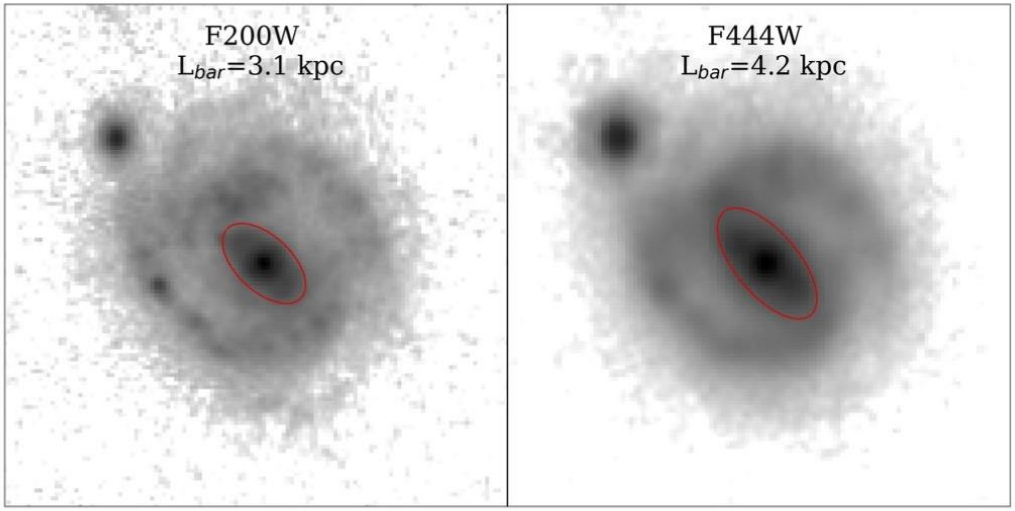

Figure 9. Single-band images of the example galaxy EGS 23205 in the NIRCam filters F200W (left) and F444W (right) at $z \approx 2.1$. The deprojected bar length is specified, and the bar is represented by a red ellipse. This galaxy is chosen to illustrate how bars are measured to be shorter in the short wavelength channels of NIRCam than in the long wavelength channels. The rest-frame wavelength is $\sim 0.645\mu m$ and $1.4\mu m$ for the two wavelengths, respectively.

Сила бара

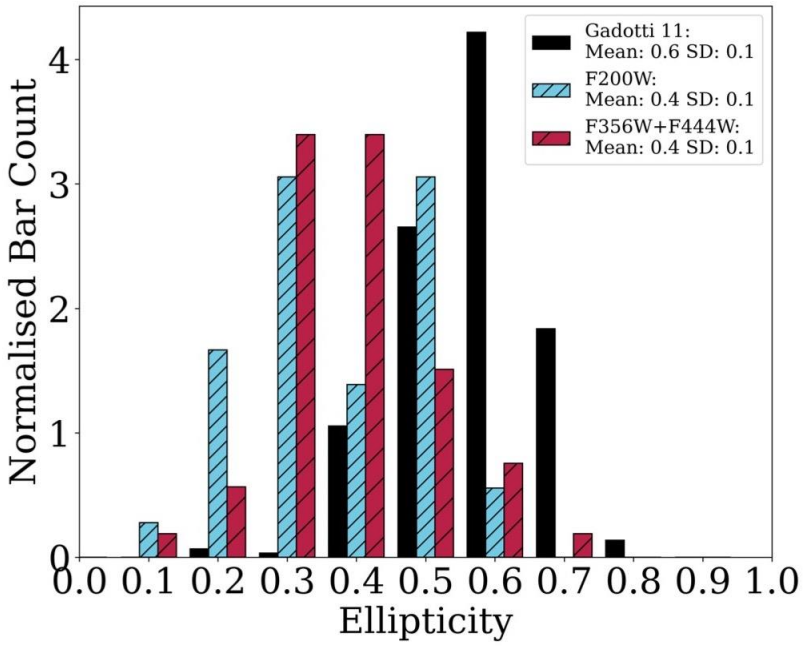

Figure 8. Distribution of the projected bar ellipticity for JWST NIRCam filters F200W (double hatched) and F356W+F444W (hatched) for bars found in galaxies in the redshift range $1 \leq z \leq 4$. The high redshift sample is compared against a sample of SDSS barred galaxies at $z \approx 0$ (G11, solid black). The mean ellipticity and standard deviation are given for each sample.

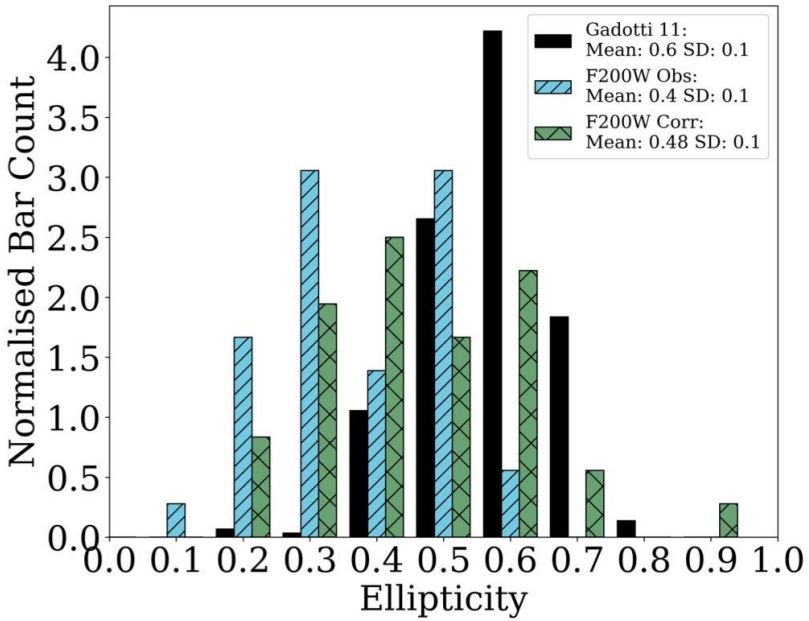

Figure 11. Distribution of the projected bar ellipticity for the JWST NIRCam filter F200W (double hatched) and corrected for resolution effects (cross hatched) for bars found in galaxies in the redshift range $1 \leq z \leq 4$. Bias-corrected bar ellipticities are derived from L24 (their Equation 4). The high redshift sample is compared against a sample of SDSS barred galaxies at $z \approx 0$ G11 (solid black). The mean ellipticity and standard deviation are given for each sample.

Выводы

- Встречаемость баров падает с красным смещением.
- Длинные бары, > 8 кпк, встречаются только на z<1; но вообще отдельного роста бара обнаружить не удалось, L_b/R остается постоянным до z=4.
- Тонкие диски, в которых развиваются бары, есть и на красных смещениях вплоть до 4!

ArXiv: 2510.08801

The Distribution of Quenched Galaxies in the Massive $z = 0.87$ Galaxy Cluster El Gordo

Rachel Honor [1], Seth H. Cohen [1], Timothy Carleton [1], S. P. Willner [2], Maria del Carmen Polletta [3], Rogier A. Windhorst [1], Dan Coe [4,5,6], Christopher J. Conselice [7], Jose M. Diego [8], Simon P. Driver [9], Jordan C. J. D'Silva [9,10], Nicholas Foo [1], Brenda L. Frye [11], Norman A. Grogin [4], Nimish P. Hathi [4], Rolf A. Jansen [1], Patrick S. Kamieneski [1], Anton M. Koekemoer [4], Reagen Leimbach [11], Madeline A. Marshall [12,10], Rafael Ortiz III [1], Nor Pirzkal [4], Massimo Ricotti [13], Aaron S. G. Robotham [9], Michael J. Rutkowski [14], Russell E. Ryan, Jr. [4], Payaswini Saikia [15], Jake Summers [1], Christopher N. A. Willmer [16] and Haojing Yan [17]

[1] *School of Earth and Space Exploration, Arizona State University, Tempe, AZ 85287-1404, USA*

[2] *Center for Astrophysics | Harvard & Smithsonian, 60 Garden Street, Cambridge, MA, 02138, USA*

[3] *INAF – Istituto di Astrofisica Spaziale e Fisica Cosmica Milano, Via A. Corti 12, I-20133 Milano, Italy*

[4] *Space Telescope Science Institute, 3700 San Martin Drive, Baltimore, MD 21218, USA*

[5] *Association of Universities for Research in Astronomy (AURA) for the European Space Agency (ESA), STScI, Baltimore, MD 21218, USA*

[6] *Center for Astrophysical Sciences, Department of Physics and Astronomy, The Johns Hopkins University, 3400 N Charles St. Baltimore, MD 21218, USA*

[7] *Jodrell Bank Centre for Astrophysics, Alan Turing Building, University of Manchester, Oxford Road, Manchester M13 9PL, UK*

[8] *Instituto de Física de Cantabria (CSIC-UC), Avda. Los Castros s/n, 39005 Santander, Spain*

[9] *International Centre for Radio Astronomy Research (ICRAR) and the International Space Centre (ISC), The University of Western Australia, M468, 35 Stirling Highway, Crawley, WA 6009, Australia*

[10] *ARC Centre of Excellence for All Sky Astrophysics in 3 Dimensions (ASTRO 3D), Australia*

[11] *Department of Astronomy/Steward Observatory, University of Arizona, 933 N. Cherry Avenue, Tucson, AZ 85721, USA*

[12] *National Research Council of Canada, Herzberg Astronomy & Astrophysics Research Centre, 5071 West Saanich Road, Victoria, BC V9E 2E7, Canada*

[13] *Department of Astronomy, University of Maryland, College Park, 20742, USA*

[14] *Department of Physics and Astronomy, Minnesota State University, Mankato, MN 56001, USA*

[15] *Center for Astrophysics and Space Science (CASS), New York University Abu Dhabi, PO Box 129188, Abu Dhabi, UAE*

[16] *Steward Observatory, University of Arizona, 933 N Cherry Ave, Tucson, AZ, 85721-0009, USA*

[17] *Department of Physics and Astronomy, University of Missouri, Columbia, MO 65211, USA*

ABSTRACT

El Gordo (ACT-CL J0102−4915) is a massive galaxy cluster with two major mass components at redshift $z = 0.87$. Using SED fitting results from JWST/NIRCam photometry, the fraction of quenched galaxies in this cluster was measured in two bins of stellar mass: $9 < \log(M_*/\mathrm{M}_\odot) < 10$ and $10 \leq \log(M_*/\mathrm{M}_\odot) < 12$. While there is no correlation between the quenched fraction and angular separation from the cluster's overall center of mass, there is a correlation between the quenched fraction and angular separation from the center of the nearest of the two mass components for the less-massive galaxies. This suggests that environmental quenching processes are in place at $z \sim 1$, and that dwarf galaxies are more affected by those processes than massive galaxies.

Для ~300 членов скопления профиттировали SED/NIRCam (8 фильтров от 0.9 до 4.5 мкм)

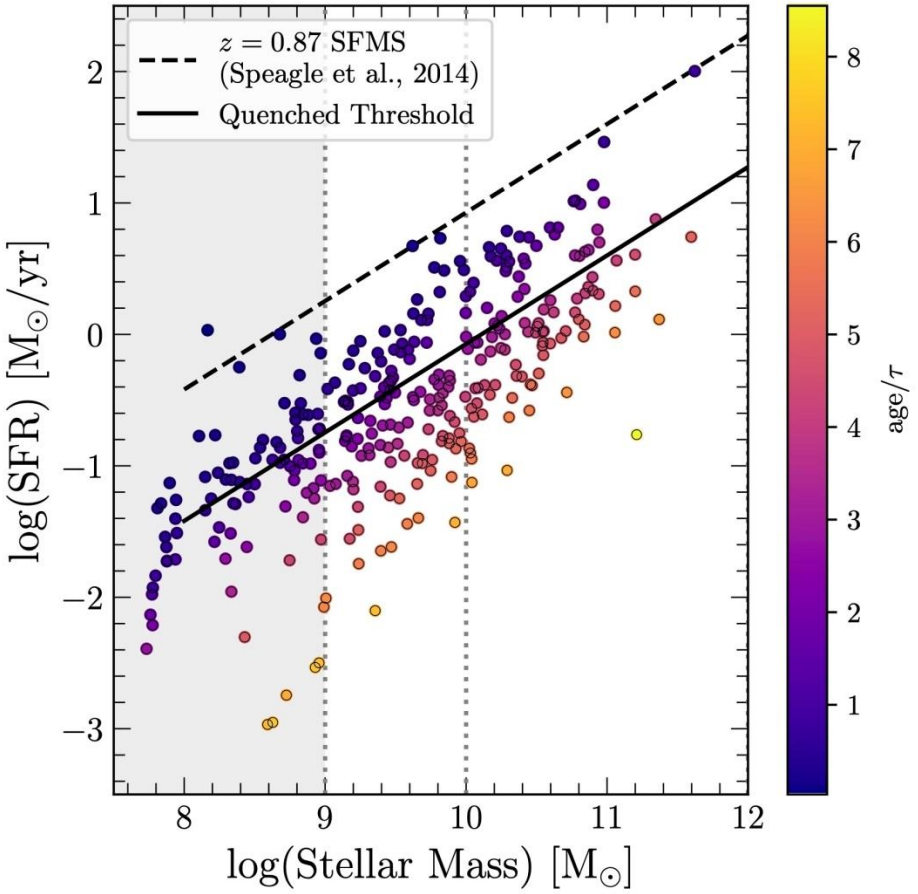

Figure 3. The parameters log(SFR) vs. log(M_*) derived by SED fits of JWST/NIRCam photometry of El Gordo cluster members. The dashed black line shows the star-formation main sequence best fit from Speagle et al. (2014) for $z = 0.87$. The solid black line is 1 dex below the SFMS, representing the quenched threshold as described by Donnari et al. (2021) and Park et al. (2023). The color represents the age/τ value for each galaxy according to the color bar on the right—as expected, galaxies with lower SFRs have older ages parameterized this way. The shaded region represents the stellar mass range in which we are incomplete, and the dotted grey lines represent the two mass bins we split the data into.

Влияние положения галактики в субскоплении на quenching

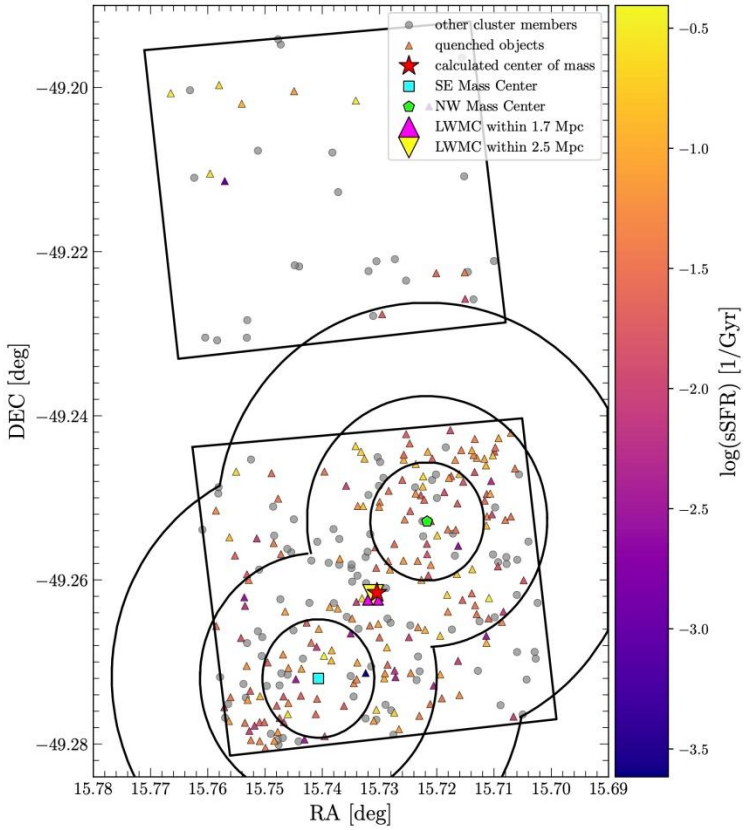

Figure 4. Positions of cluster galaxies. Quenched objects are shown as triangles with colors indicating specific SFR as shown on the color bar to the right of the plot. The grey circles mark the other (i.e., not quenched) cluster galaxies. The cyan square and green pentagon mark the southeast and northwest mass centers, respectively, and the pink and yellow triangles mark the luminosity-weighted mass centers (LWMCs) within 1.7 and 2.5 Mpc (Frye et al. 2023). The red star marks the center of mass as computed using the Bagpipes stellar masses of the cluster objects in Module B. The regions separated by black lines represent the three regions where quenched fraction was measured. The circles are centered on the mass centers and have radii 26″, 55″, and 96″.

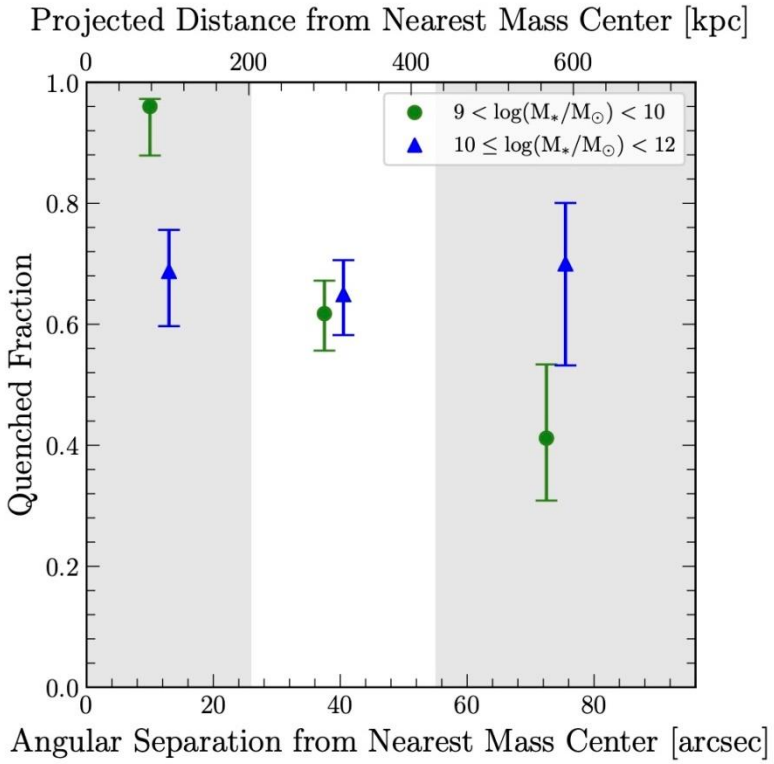

Figure 5. The quenched fraction of galaxies in El Gordo as a function of distance to the nearest mass center. Colored points show the quenched fractions within 3 angular separation bins from the nearest mass center. Angular separation from the nearest mass center is given in arcseconds on the bottom axis, and proper distance from the nearest mass center is given in kiloparsecs on the top axis. The sample is separated into $9 < \log(M_*/\mathrm{M}_\odot) < 10$ (green circles), and $10 \leq \log(M_*/\mathrm{M}_\odot) < 12$ (blue triangles). Shading indicates the boundaries between different regions.

Подавление звездообразования в скоплениях – в контексте

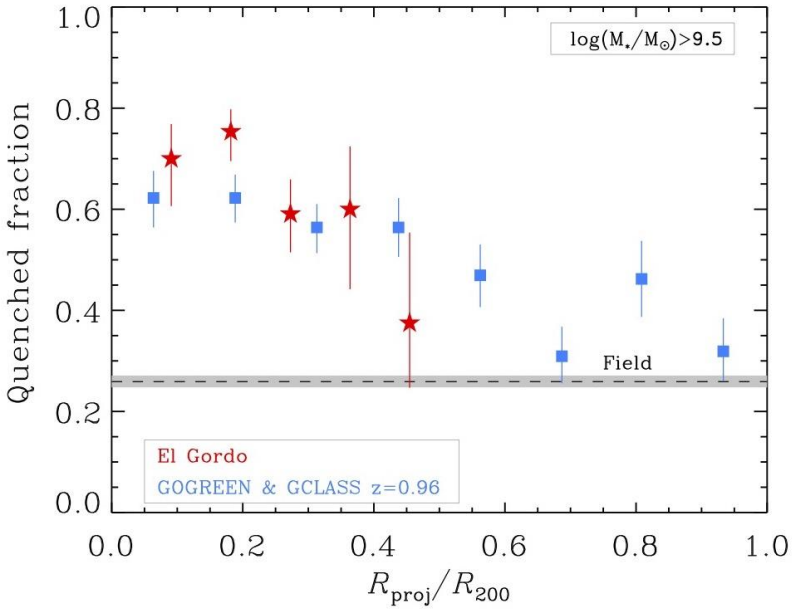

Figure 6. Quenched fraction compared to other clusters. The horizontal axis is the projected distance to the cluster mass center (nearest of the two mass centers, for El Gordo) normalized to R_{200}, and all galaxies have $\log(M_*/\mathrm{M}_\odot) > 9.5$. Red stars show measurements of the quenched fraction of galaxies in El Gordo, and blue squares show the quenched fractions for a sample of clusters from the GOGREEN and GCLASS surveys at $0.867 < z < 1.12$ ($\langle z \rangle = 0.96$) (Hewitt et al. 2025). The dashed black line shows the quenched fraction for field galaxies Martis et al. (2016) at $z = 0.75$–1.0 and with $M_* > 10^{9.4}\,\mathrm{M}_\odot$.

4.3. *Quenched Galaxy Fraction vs. Redshift*

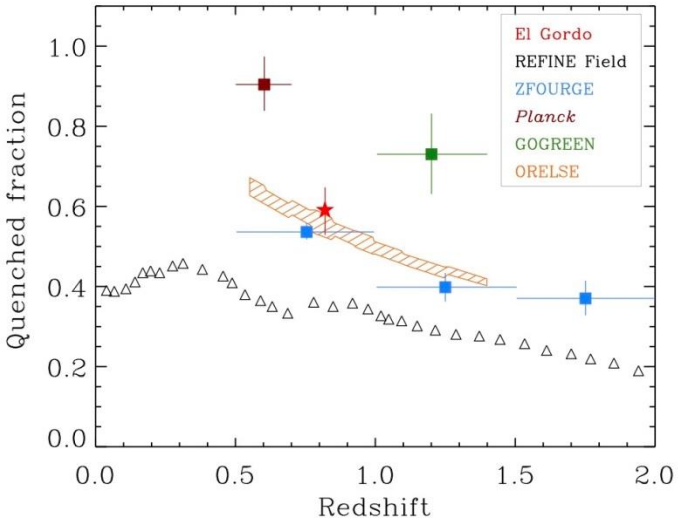

Figure 7. Quenched fraction for massive galaxies in El Gordo compared to galaxies in other clusters. All comparisons are for galaxies with $10.25 < \log(M_*/\mathrm{M}_\odot) < 11$ and $R/R_{200} < 0.5$. El Gordo is shown as a red star. The other symbols refer to galaxies from the field derived in the REFINE survey (black open triangles; Sarron & Conselice 2021), from the ZFOURGE group sample (full blue squares; Papovich et al. 2018; Straatman et al. 2016), from the ORELSE cluster sample (orange hatched region; Lubin et al. 2009; Straatman et al. 2016), from the *Planck* cluster sample at $0.5 < z < 0.7$ (full maroon square; van der Burg et al. 2018), and from the the GOGREEN cluster sample (full green square; van der Burg et al. 2020; Balogh et al. 2017).

Механизмы quenching'а?

- Внутренние – для массивных галактик
- Внешние для маломассивных галактик…
- Но не ram pressure! Потому что в NW-концентрации El Gordo рентген не наблюдается.